Supporting information for

Unusual Electronic Effects Imparted by Bridging Dinitrogen: an Experimental and Theoretical Investigation

*Wesley A. Hoffert, Anthony K. Rappé, and Matthew P. Shores**

Department of Chemistry, Colorado State University, Fort Collins, CO 80523–1872

Additional Electrochemical Information

Electrochemical assignments have been confirmed by agitation experiments whereby the voltammograms were collected while stirring the samples (Figure S1). In the cyclic voltammograms for **1** and **2**, there is also a further irreversible two electron oxidation at –0.31 V for **1** and –0.34 V for **2** (Figure S2). Additional support for all assignments are supported by electrochemical simulations performed for **1** (Figure S3). Electrochemical investigations confirm that the oxidized complexes maintain the same solution structure as the neutral parent species. Cyclic voltammetry of **4** performed at –40 °C in tetrahydrofuran shows the presence of two redox events at nearly the same potentials as observed for **2**. However, agitation experiments demonstrate that these waves are assignable to stepwise *reductions* from Cr(II) to Cr(I) (Figure S1). Early cyclic voltammograms of **3** were performed in diethyl ether because adventitious chloride (from LiCl) was relatively benign in that solvent compared to tetrahydrofuran: in THF, solutions of **3** contaminated with LiCl led to the formation of $[(^{i}Pr_3SiC_2)(dmpe)_2Cr^{III}Cl](BAr_4^F)$ after standing for minutes. However, extraction of neutral **2** followed by filtration through Celite allowed for complete removal of chloride; batches of **3** synthesized from **2** following this workup are stable in THF for days. Nonetheless, the cyclic voltammetry data reported below were collected prior to adoption of the Celite protocol, and were taken in diethyl ether at –40 °C (with $(TBA)(BAr^F_4)$ as an electrolyte. The CV for **3** shows two one-electron redox waves at –1.15 V and – 1.70 V, very close to the waves observed for **2** (–1.34 V and –1.55 V) considering the change in solvent. Further support for the mixed-valent nature of **3** is found by investigating the electrochemistry during agitation: the wave at –1.15 V is designated as an oxidation from Cr(I) to Cr(II) while the redox event at –1.70 V is assignable as a reduction from Cr(II) to Cr(I) (Figure S4).

Figure S1. Cyclic voltammograms for (a) 2 and (b) 4 obtained while the samples were stirred. In (a), high amplitude noise at potentials positive of the redox process indicate an oxidation. In (b), high amplitude noise at potentials more negative than the redox potential suggests a reduction event.

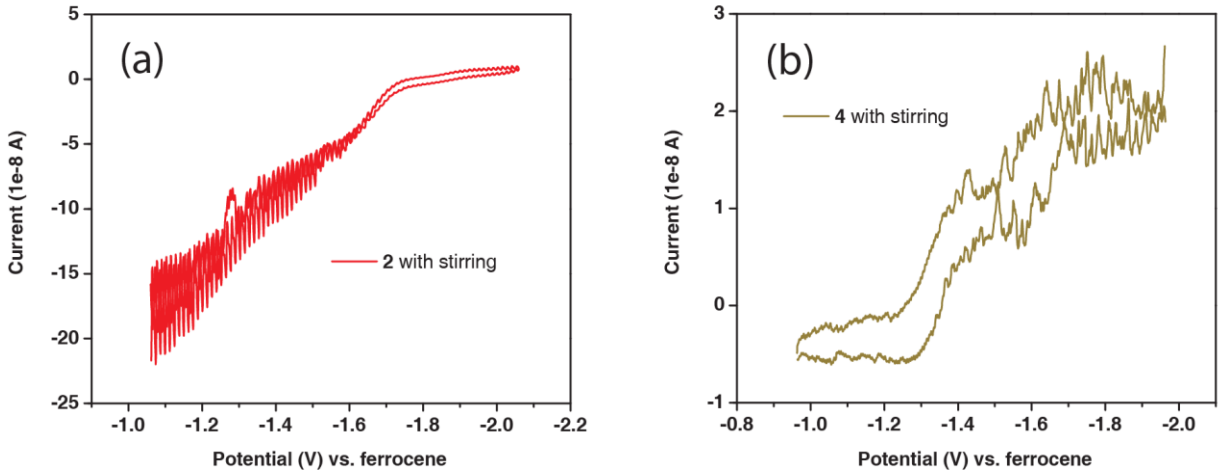

Figure S2. Full cyclic voltammograms for **1** (black trace) and **2** (red trace).

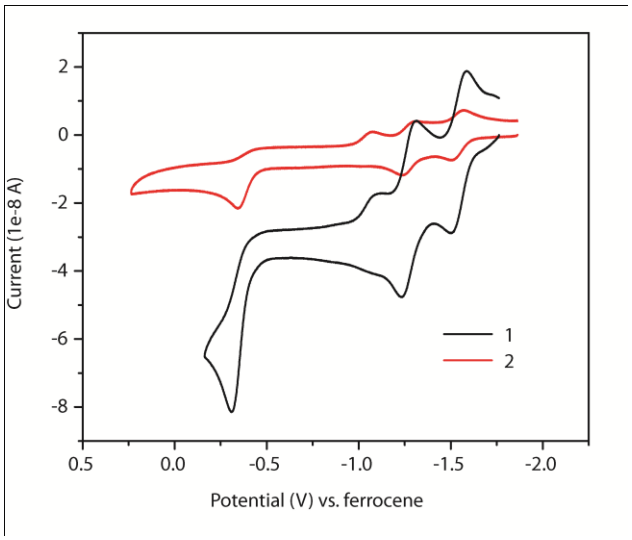

Figure S3. Simulated (red trace) and experimentally determined (black trace) cyclic voltammograms for **1**. Redox events shown between −1 and −1.6 V were modeled as one electron processes. The wave at ca. −0.3 V was modeled as an irreversible two electron oxidation. The appearance of the third wave at ca. −1.1 V is a result of the irreversible oxidation. The simulation was created using BASi DigiSim 3.03b software[1] and was modeled at a scan rate of 0.1 V/s.

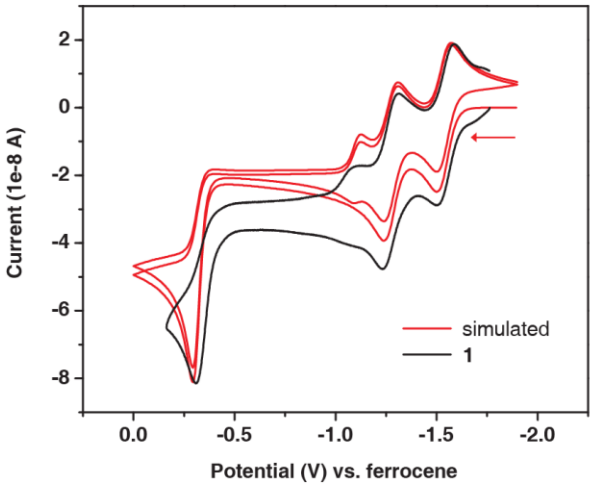

[1] *DIGISIM*, Bioanalytical Systems, Inc.: West Lafayette, IN, 2004.

Figure S4. Electrochemical behavior for **3** in (a) static solution and (b) while stirring. Both voltammograms were recorded in 0.1 M solutions of (TBA)(BAr^F_4) in diethyl ether at −40°C with a 4 mm diameter glassy carbon working electrode. The reference and auxiliary electrodes are described in the main text. In (b), high amplitude noise at potentials more positive than the redox event at −1.15 V suggests an oxidation, while noise at potentials more negative than the redox wave at −1.70 V indicates a reduction. The small peak at −1.37 V arises from an impurity that grows in intensity as the sample is warmed to room temperature (see discussion above on page S2).

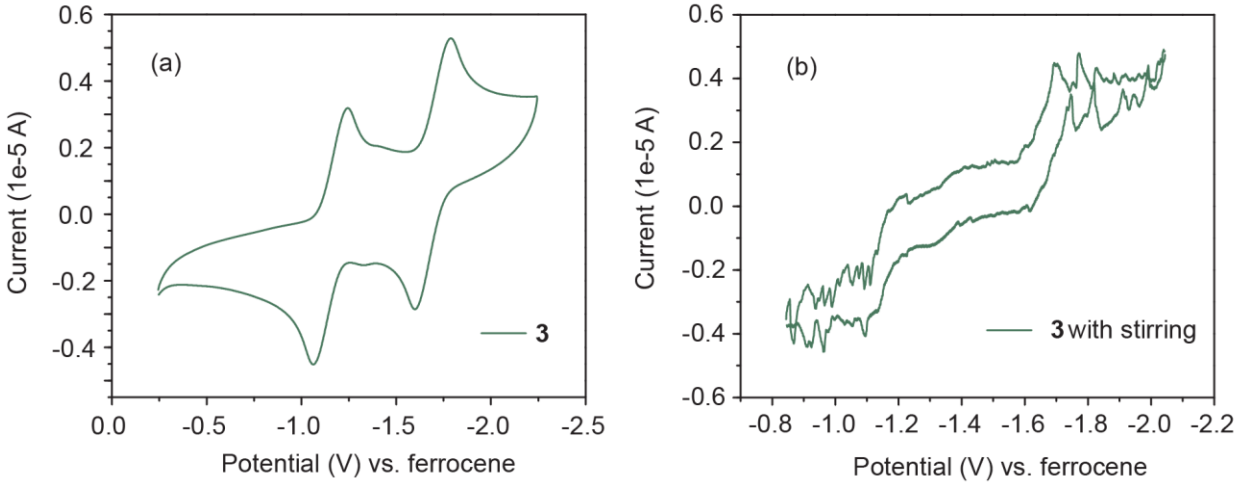

Figure S5. ^{1}H NMR spectrum of 1 taken in C_6D_6 at ambient temperature with a 300 MHz spectrometer (see experimental section in text). A minimum of 512 transients were recorded with an acquisition time of 0.5 s per transient with no acquisition delay time.

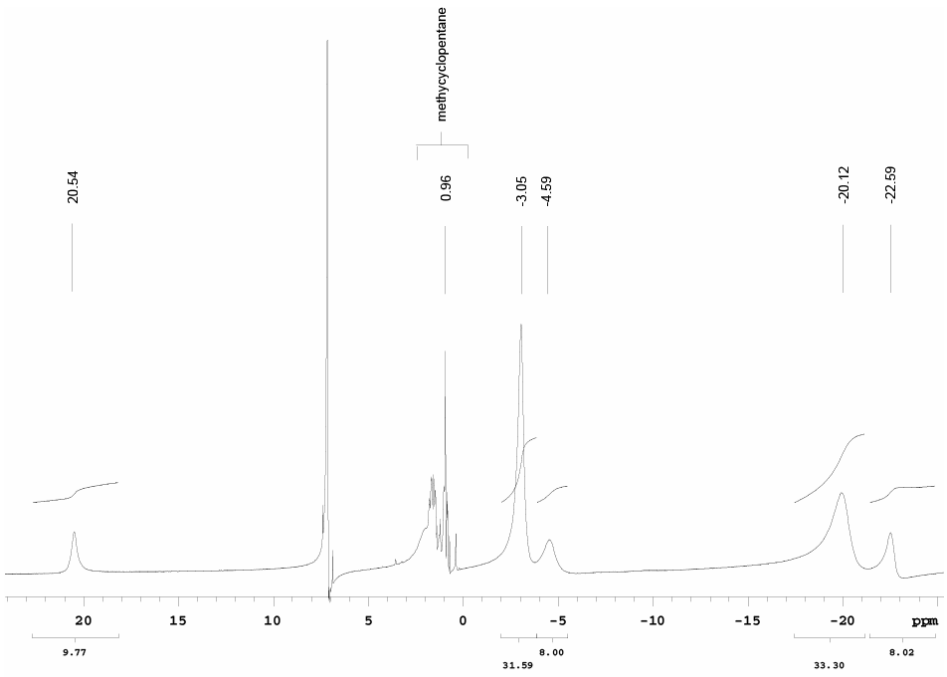

Figure S6. ^{1}H NMR spectrum of **2** taken in C_6D_6 at ambient temperature with a 300 MHz spectrometer (see experimental section in text). A minimum of 512 transients were recorded with an acquisition time of 0.5 s per transient with no acquisition delay time.

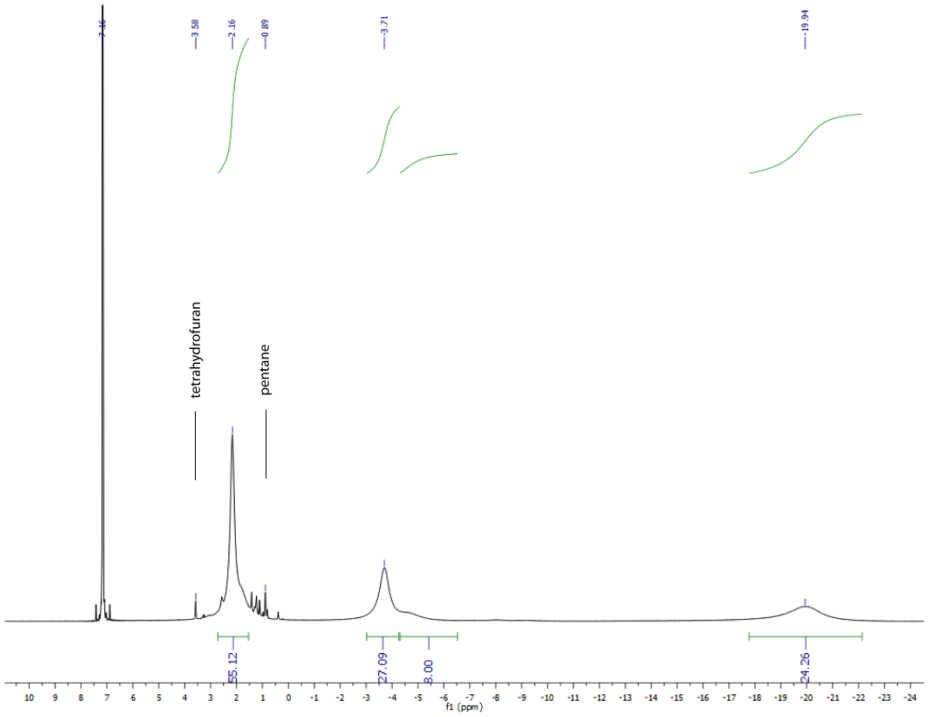

Figure S7. Vis-NIR spectrum of **3** in diethyl ether. The peak at ca. 11000 cm^{-1}corresponds to the absorption at 914 nm in the UV-Visible spectrum obtained (see manuscript).

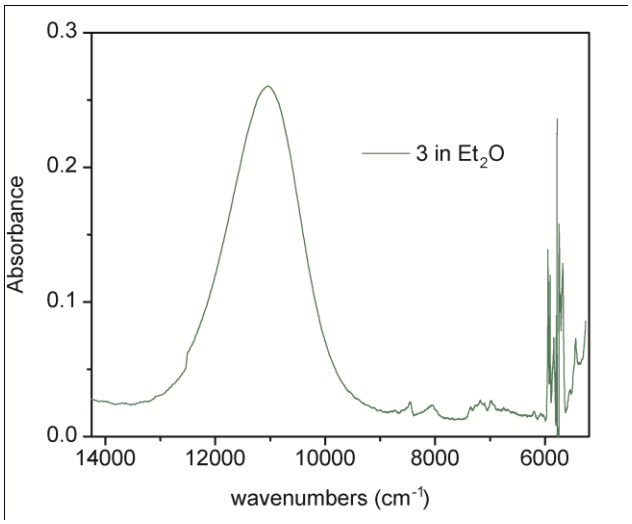

Figure S8. Temperature dependence of the magnetic susceptibility and (ferromagnetic) fit for compound **1**. Ferromagnetic fits were generated by assuming a single spin system was present. In this scenario, the downturn in susceptibility was reproduced by incorporating a zero-field splitting parameter (D) into the error minimization and allowing g, D, and TIP to refine. The best fit was obtained using julX with $S = 1$, $g = 2.01$, $D = +7.3$, TIP = 714×10^{-6} emu. Relative error (f) = 0.015.

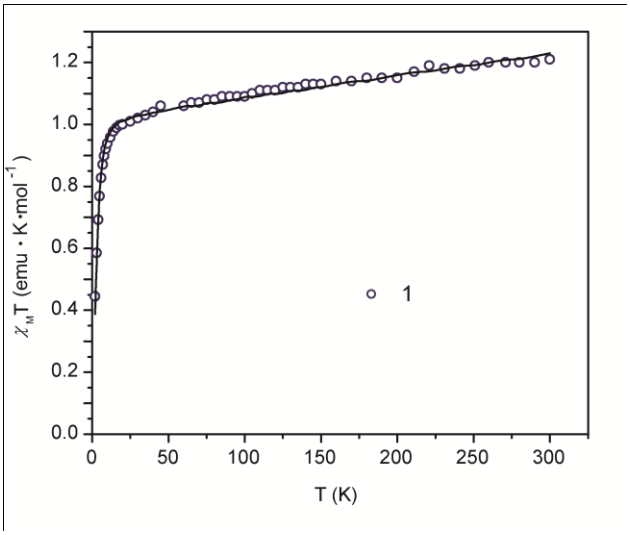

Figure S9. Magnetization behavior for **3** (top left) and **4** (top right). Below, expanded view of the magnetization behavior of **3**. Lines between data points (i.e. not the Brillouin functions) are guides to the eye only.

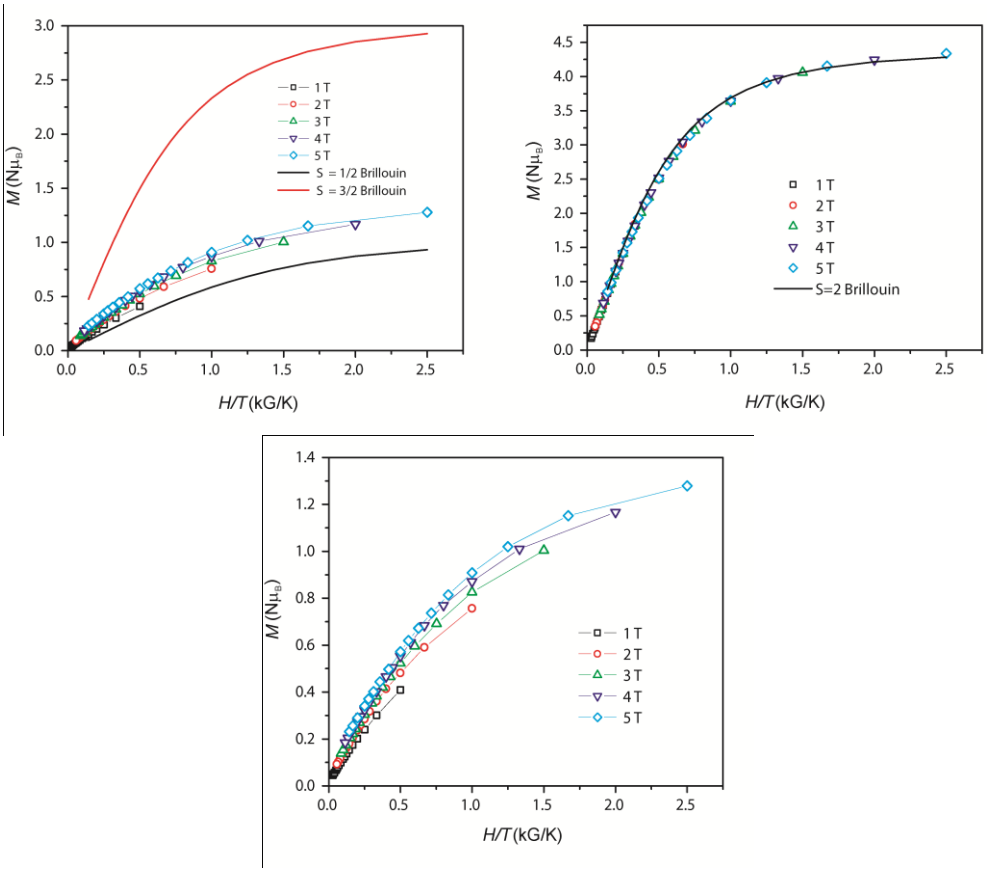

Table S1. Antiferromagnetic (AF) fits to the DC susceptibility data for complexes **1**, **2**, **3**, and **4**. The AF fits were generated by assuming two independent spin centers were present in the molecule. No zero-field splitting parameter was included in the refinement, but temperature dependent susceptibility behavior could be reproduced by allowing an exchange parameter (*J*) to refine freely along with *g* and TIP. For each fit, the g values for each Cr center were forced to be equal. The *g* values listed below are all significantly higher than the Landé *g* value of 2.0023 in addition to being inconsistent for redox-related **2-4**, which is unusual for early transition metal ions. In the AF fit for **3**, the *J* value obtained is unreasonably high when compared alongside the other complexes, and TIP values for all complexes range seem either unreasonably low or high. Fixing the TIP value at an acceptable level (ca. 400 $\times 10^{-6}$ emu) resulted in poorer fits.

	Data Range (K)	*g*	*J* (cm^{-1})	TIP (1×10^{-6} emu)	Relative error
AF model for **1**	2-300	2.36	–1.4	590	0.011
AF model for **2**	2-300	2.33	–1.6	0.0	0.015
AF model for **3**	18-300	2.38	–130	1800	0.027
AF model for **4**	2-300	2.46	–0.04	1.3	0.033

Full Reference 44 from paper:

Frisch, M. J.; Trucks, G. W.; Schlegel, H. B.; Scuseria, G. E.; Robb, M. A.; Cheeseman, J. R.; Montgomery, J., J. A. ; Vreven, T.; Kudin, K. N.; Burant, J. C.; Millam, J. M.; Iyengar, S. S.; Tomasi, J.; Barone, V.; Mennucci, B.; Cossi, M.; Scalmani, G.; Rega, N.; Petersson, G. A.; Nakatsuji, H.; Hada, M.; Ehara, M.; Toyota, K.; Fukuda, R.; Hasegawa, J.; Ishida, M.; Nakajima, T.; Honda, Y.; Kitao, O.; Nakai, H.; Klene, M.; Li, X.; Knox, J. E.; Hratchian, H. P.; Cross, J. B.; Bakken, V.; Adamo, C.; Jaramillo, J.; Gomperts, R.; Stratmann, R. E.; Yazyev, O.; Austin, A. J.; Cammi, R.; Pomelli, C.; Ochterski, J. W.; Ayala, P. Y.; Morokuma, G. A.; Voth, G. A.; Salvador, P.; Dannenberg, J. J.; Zakrzewski, V. G.; Dapprich, S.; Daniels, A. D.; Strain, M. C.; Farkas, O.; Malick, D. K.; Rabuck, A. D.; Raghavachari, K.; Foresman, J. B.; Ortiz, J. V.; Cui, Q.; Baboul, A. G.; Clifford, S.; Cioslowski, J.; Stefanov, B. B.; Liu, G.; Liashenko, A.; Piskorz, P.; Komaromi, I.; Martin, R. L.; Fox, D. J.; Keith, T.; Al-Laham, M. A.; Peng, C. Y.; Nanayakkara, A.; Challacombe, M.; Gill, P. M. W.; Johnson, B.; Chen, W.; Wong, M. W.; Gonzalez, C.; Pople, J. A. *Gaussian 03*; Gaussian, Inc.: Wallingford, CT, 2004.

Figure S10. Weiss plots for 1 (a), 2 (b), 3 (c), and 4 (d). Linear regressions were calculated from data taken between 100 and 300 K. The Curie constants for **1** and **2** are 1.3 and 1.0 $cm^3 \cdot K \cdot mol^{-1}$, respectively. For **4**, the Curie constant was found to be 3.1 $cm^3 \cdot K \cdot mol^{-1}$.

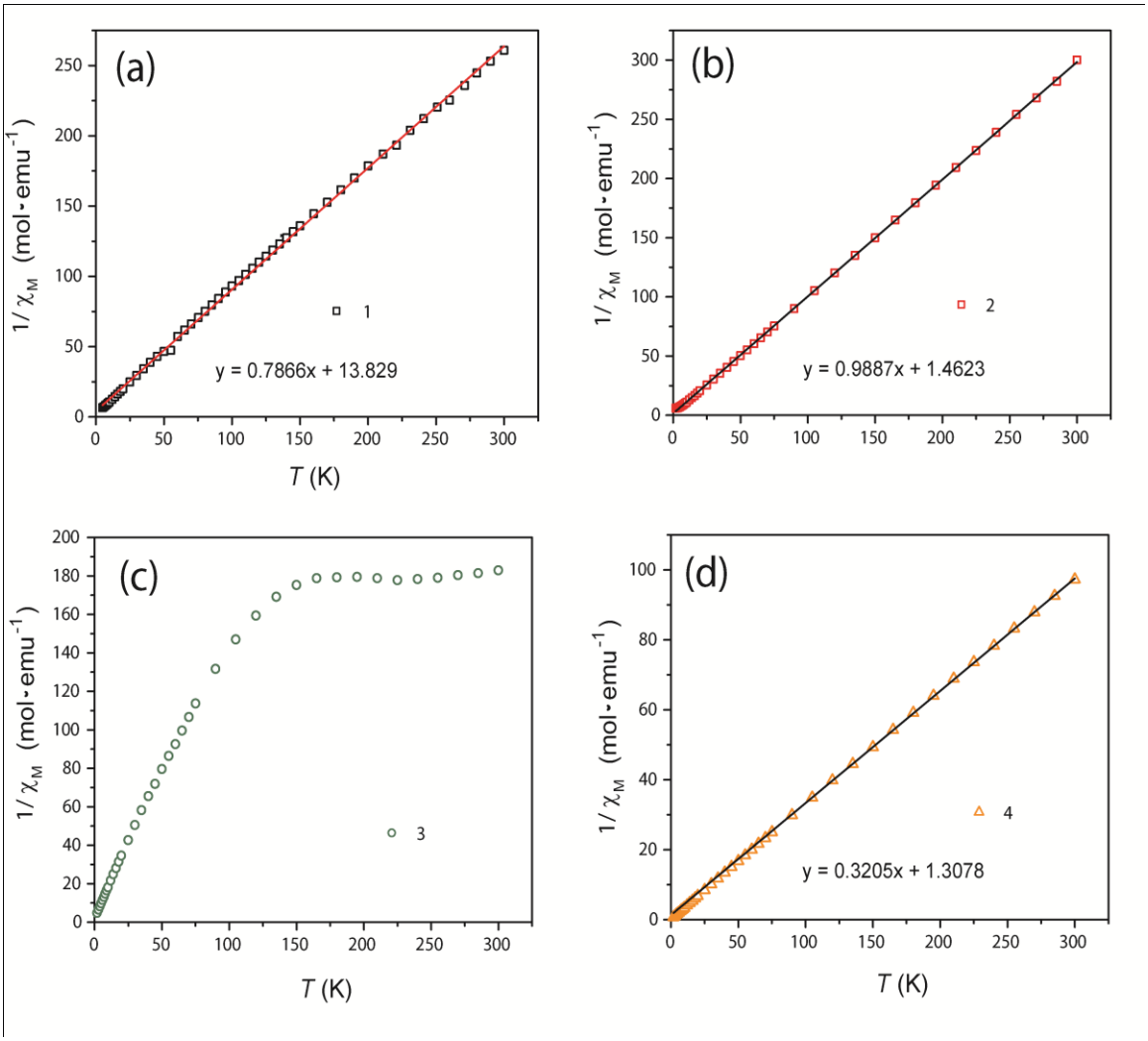

Figure S11. Solid state (top; S/N = 1.5 @ 293K, 1.8 @ 105K) and methylcyclopentane solution/glass (bottom; S/N = 1.7 @ 293 K, 2.1 @ 105 K) X-band EPR spectra of **2**. For comparison, the signal to noise ratio for solid **3** is 437.7 at 105 K and is 13 at 293 K.

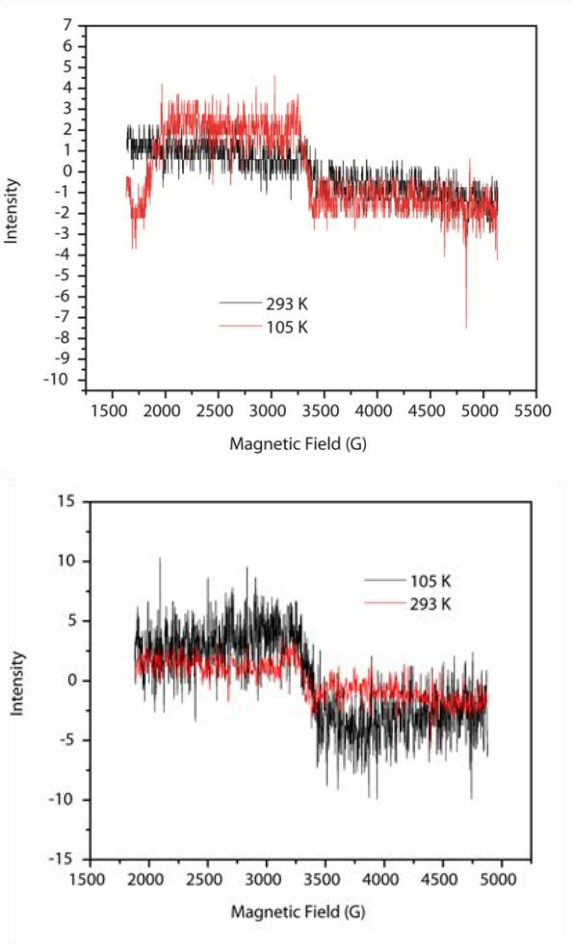

Figure S12. Solid state X-band EPR spectra for **4** at 105 K (S/N = 20) and 293 K (S/N = 13).

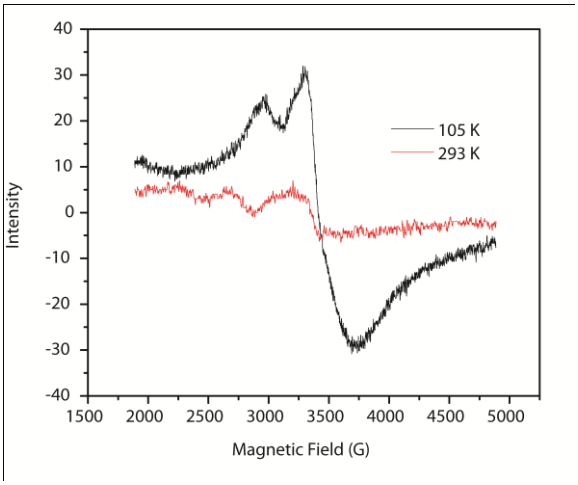

Figure S13. Full structure of **1**·C_6H_{12} with thermal ellipsoids at 40% probability. The greatest deviation from 180° along the spine any of the molecules is 5° for one of the C≡C–Ph angles in **1**.

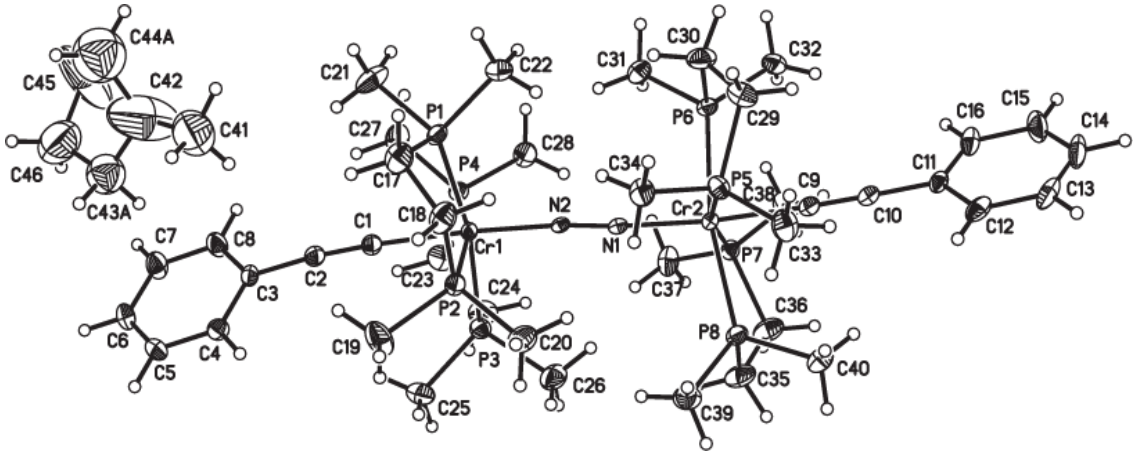

Figure S14. Full structure of **2** with thermal ellipsoids at 40% probability.

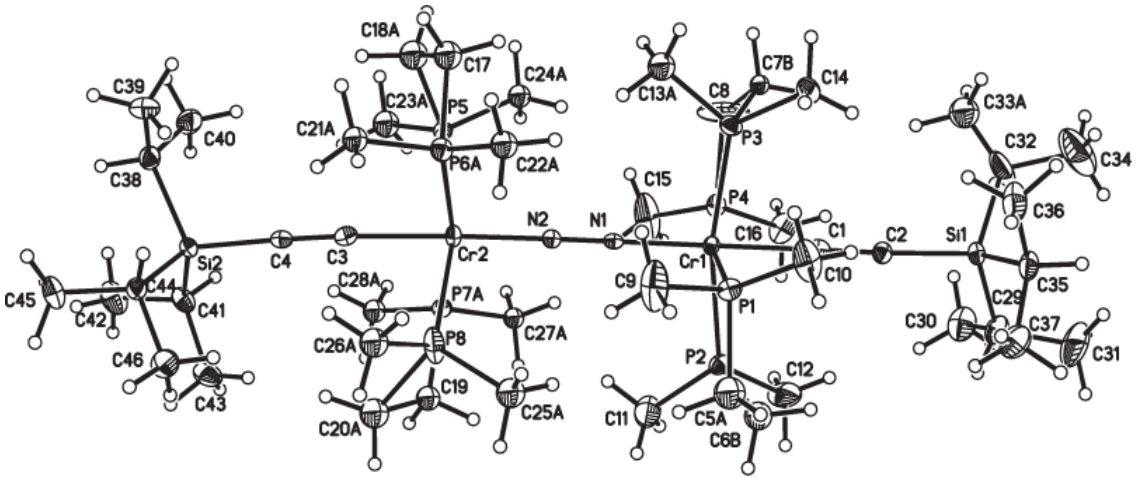

Figure S15. Full structure of **3**·1.5 Et_2O (100 K) with thermal ellipsoids at 40% probability.

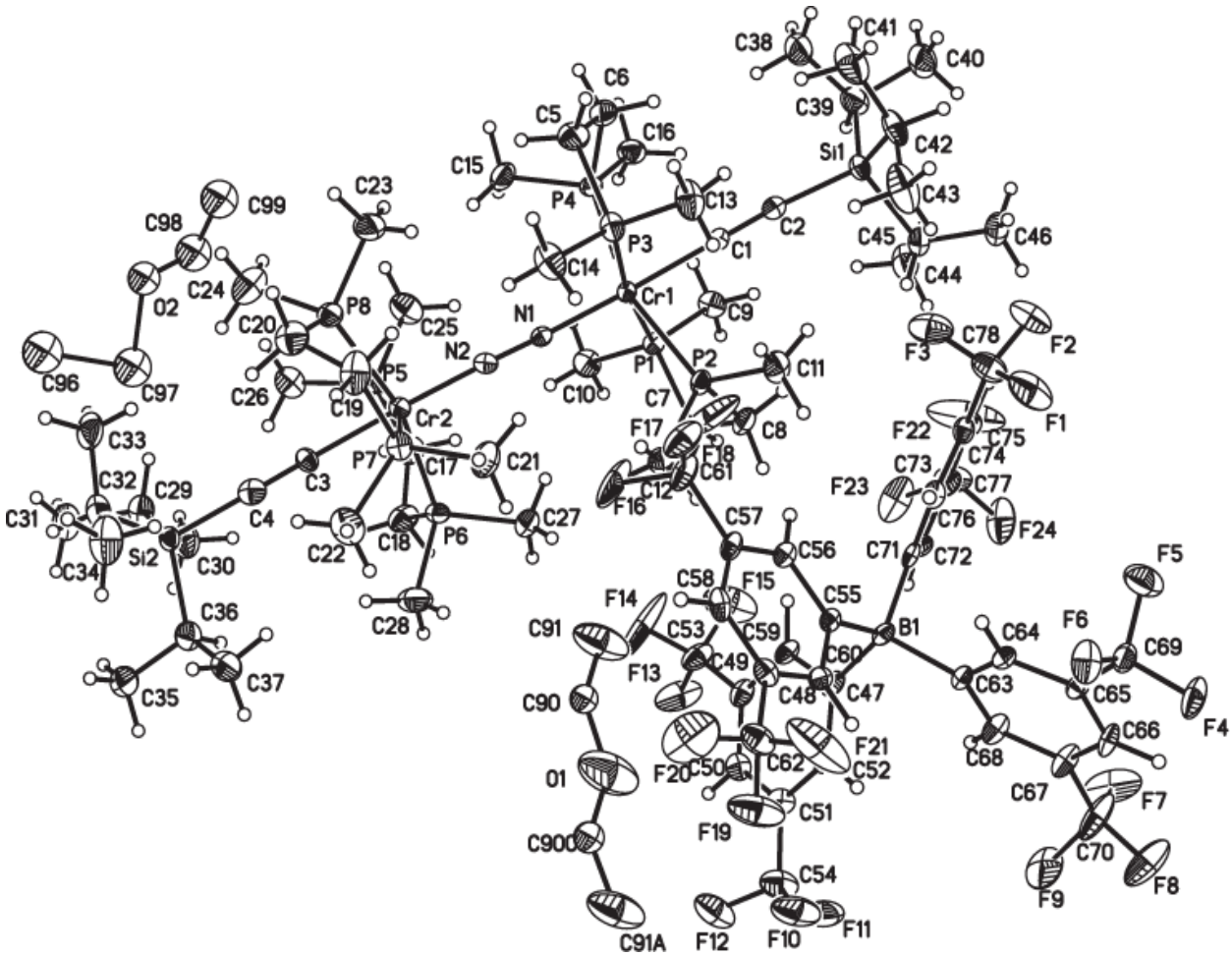

Figure S16. Full structure of **3** (296 K) with thermal ellipsoids at 40% probability.

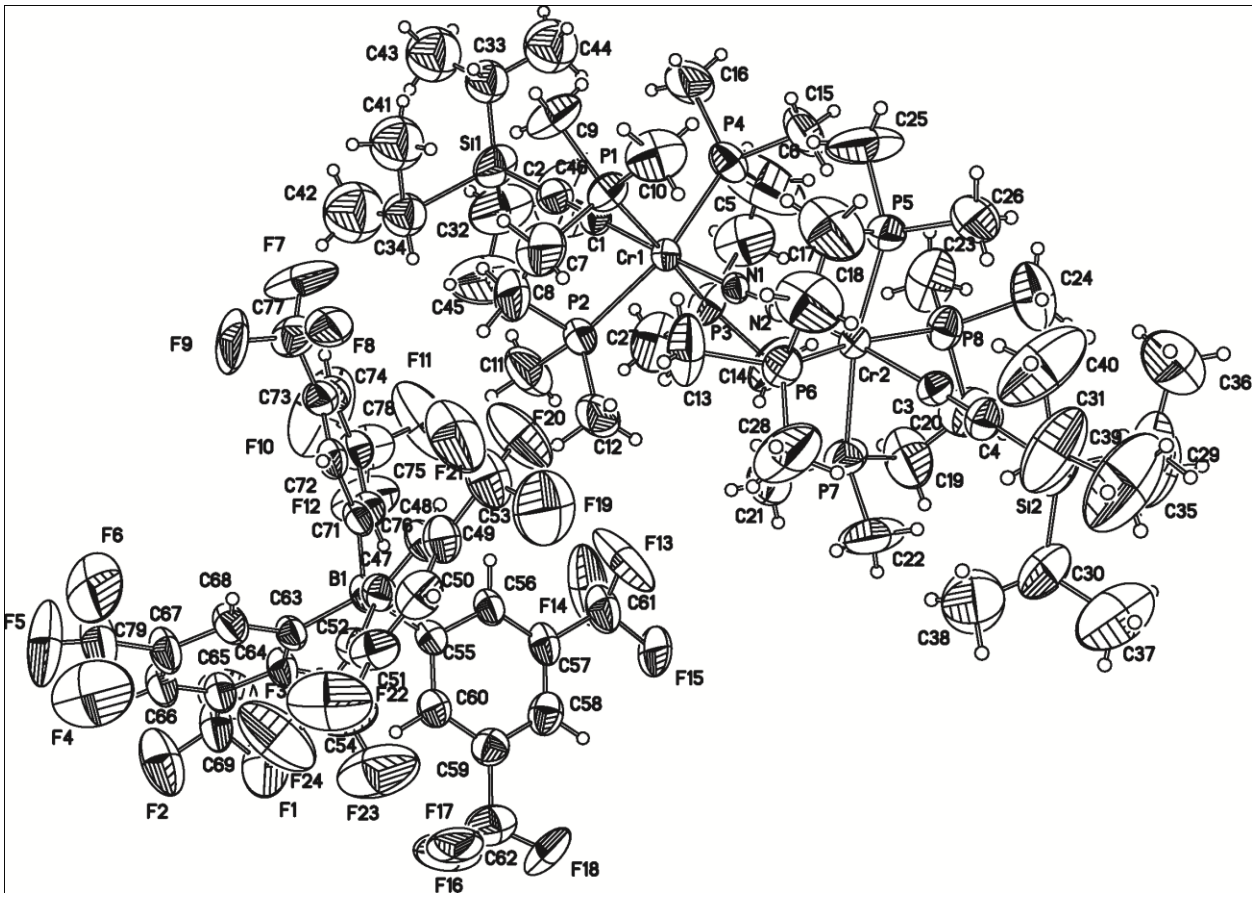

Figure S17. Full structure of **4**·3.5 THF with thermal ellipsoids at 40% probability.

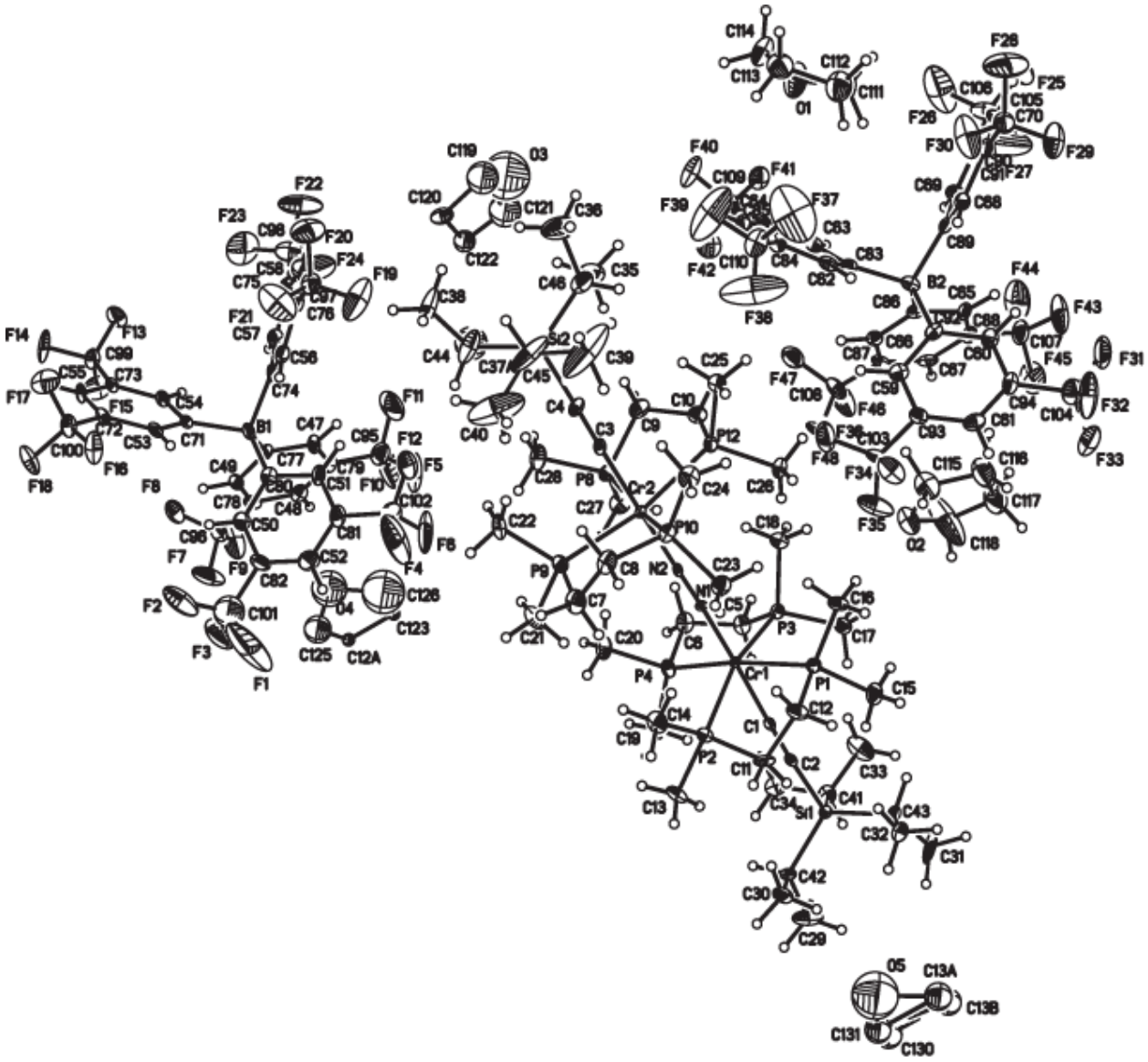

Figure S18. UKS frontier natural orbitals for **4** with corresponding electron occupancies.

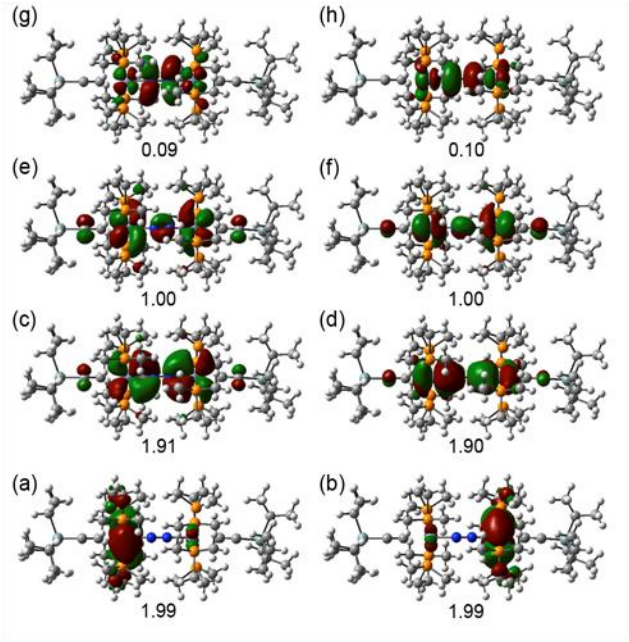

Table S2. B3LYP computed structure and total energy for $Cr^{I}Cr^{I}$ complex **2**.
E= –2158.55848834763

#	atom	x	y	z
1	Cr	2.50885	0.06566	0.01294
2	Cr	-2.48	0.04921	0.00485
3	Si	7.69737	-0.1629	-0.0597
4	Si	-7.6752	-0.0366	-0.0421
5	P	2.63031	-1.0413	2.21039
6	P	2.83002	-2.2545	-0.8155
7	P	2.83102	2.37185	0.86061
8	P	2.7022	1.19098	-2.1835
9	P	-2.7994	2.23329	-1.1092
10	P	-2.8046	-2.1483	1.10572
11	N	0.60815	0.07375	0.00911
12	N	-0.5814	0.06784	0.02096
13	C	4.61996	0.02604	0.02741
14	C	5.86342	-0.0266	0.01693
15	C	-4.5908	0.0149	-0.0335
16	C	-5.835	-0.0128	-0.0496
17	C	2.69478	3.0858	-1.8874
18	C	1.22	-0.9383	3.462
19	H	1.27928	-1.7448	4.20171
20	H	0.268	-0.9862	2.93024
21	H	1.2756	0.02204	3.98234
22	C	4.0955	-0.795	3.37773
23	H	4.0572	0.21303	3.79971
24	H	5.01889	-0.8903	2.80503
25	H	4.07591	-1.5268	4.19286
26	C	1.4266	-3.3844	-1.405
27	H	1.14897	-3.1131	-2.4268
28	H	0.55021	-3.2521	-0.7677
29	H	1.73552	-4.4355	-1.3908
30	C	4.1204	-2.693	-2.1227
31	H	4.31401	-3.7714	-2.1402
32	H	5.03917	-2.1518	-1.8903
33	H	3.76154	-2.3814	-3.1086
34	C	4.14257	2.79837	2.15236
35	H	5.04711	2.23152	1.92373
36	H	3.78236	2.51173	3.14512
37	H	4.36183	3.87192	2.15185
38	C	1.40827	1.06868	-3.5567
39	H	1.54864	1.85893	-4.3028
40	H	0.411	1.14348	-3.1202
41	H	1.49575	0.09635	-4.0498
42	C	4.26461	1.02937	-3.2353
43	H	4.26455	1.76416	-4.0481
44	H	4.31194	0.02329	-3.6609
45	H	5.13633	1.16944	-2.5944
46	C	8.14804	-1.4713	-1.4207
47	H	7.49724	-2.3294	-1.1946
48	C	7.79592	-0.994	-2.8404
49	H	8.43304	-0.1554	-3.1498
50	H	6.75506	-0.6627	-2.914
51	H	7.94494	-1.7992	-3.5736
52	C	9.60221	-1.9758	-1.3771
53	H	9.7515	-2.7883	-2.1021
54	H	9.88424	-2.3609	-0.391
55	H	10.3132	-1.1824	-1.6374
56	C	8.4724	1.55151	-0.5314
57	H	8.32351	1.63299	-1.6189
58	C	9.98843	1.63581	-0.2696
59	H	10.3904	2.59459	-0.6261
60	H	10.5474	0.83988	-0.7735
61	H	10.2171	1.56957	0.80141
62	C	8.40551	-0.8016	1.62199
63	H	9.4946	-0.8721	1.48143
64	C	8.15245	0.15868	2.7976
65	H	7.08043	0.33507	2.94591
66	H	8.62767	1.13342	2.64166
67	H	8.55171	-0.2558	3.73422
68	C	7.88977	-2.2131	1.95769
69	H	8.32106	-2.5745	2.90188
70	H	8.14158	-2.9435	1.18005
71	H	6.79893	-2.2185	2.07099
72	C	-8.3719	1.76693	-0.0803
73	H	-9.464	1.66229	0.00126
74	C	-7.8969	2.60222	1.12158
75	H	-8.3419	3.60701	1.10297
76	H	-6.8067	2.72353	1.10736
77	H	-8.1631	2.14207	2.0806
78	C	-8.0768	2.50774	-1.3956
79	H	-8.5074	3.51895	-1.3797
80	H	-8.4923	1.98896	-2.2671
81	H	-6.9975	2.61373	-1.5575
82	C	-8.302	-0.9326	-1.6405

Table S3. B3LYP Computed structure and total energy for $Cr^{II}Cr^{II}$ complex in **4**.
E= -2158.20795932198

#	atom	x	y	z	#	atom	x	y	z
1	Cr	2.509725	0.066187	0.01321	42	C	4.304259	1.00316	-3.27249
2	Cr	-2.48521	0.030722	0.007084	43	H	4.319935	1.734301	-4.08666
3	Si	7.669346	-0.15816	-0.07471	44	H	4.349247	-0.00312	-3.69516
4	Si	-7.65079	-0.01904	-0.04113	45	H	5.164873	1.14157	-2.61777
5	P	2.679823	-1.03823	2.301193	46	C	8.080689	-1.5027	-1.40515
6	P	2.876547	-2.32596	-0.81145	47	H	7.401892	-2.33964	-1.17915
7	P	2.864838	2.450968	0.865418	48	C	7.781624	-1.03623	-2.84136
8	P	2.729473	1.197192	-2.26789	49	H	8.460711	-0.23225	-3.14918
9	P	-2.84569	2.258472	-1.18053	50	H	6.757355	-0.66213	-2.95367
10	P	-2.85499	-2.20726	1.186399	51	H	7.916549	-1.86017	-3.55398
11	N	0.603849	0.063497	0.008788	52	C	9.519875	-2.0484	-1.31729
12	N	-0.58168	0.050095	0.018762	53	H	9.661083	-2.86624	-2.03533
13	C	4.561827	0.033644	0.021002	54	H	9.763099	-2.44016	-0.32429
14	C	5.801091	-0.02443	0.002927	55	H	10.26069	-1.27852	-1.56035
15	C	-4.53737	0.008172	-0.02712	56	C	8.392237	1.557505	-0.59346
16	C	-5.77769	-0.00776	-0.04356	57	H	8.194751	1.632111	-1.67335
17	C	2.703012	3.065352	-1.9068	58	C	9.920236	1.635033	-0.39968
18	C	1.248001	-0.9482	3.517889	59	H	10.30425	2.594027	-0.76971
19	H	1.337074	-1.72814	4.280964	60	H	10.45205	0.843227	-0.93693
20	H	0.306259	-1.05927	2.977404	61	H	10.19923	1.561727	0.658439
21	H	1.25644	0.026456	4.012695	62	C	8.341563	-0.75305	1.630884
22	C	4.148371	-0.70296	3.421547	63	H	9.426872	-0.85008	1.483794
23	H	4.053774	0.291435	3.864078	64	C	8.126723	0.25001	2.778116
24	H	5.062711	-0.73695	2.829819	65	H	7.062237	0.466063	2.936725
25	H	4.186023	-1.44667	4.223324	66	H	8.631796	1.202895	2.590408
26	C	1.465409	-3.47759	-1.30229	67	H	8.523451	-0.14926	3.720513
27	H	1.103437	-3.20817	-2.29739	68	C	7.807275	-2.14672	2.010879
28	H	0.640404	-3.38472	-0.59331	69	H	8.248998	-2.48775	2.955901
29	H	1.811203	-4.51589	-1.32492	70	H	8.035504	-2.90261	1.251341
30	C	4.122708	-2.68216	-2.16934	71	H	6.717758	-2.13394	2.146166
31	H	4.364446	-3.74932	-2.18746	72	C	-8.285	1.798922	0.073504
32	H	5.024614	-2.099	-1.98084	73	H	-9.38052	1.708568	0.099231
33	H	3.70165	-2.40143	-3.13888	74	C	-7.8547	2.512824	1.366454
34	C	4.172554	2.808138	2.165743	75	H	-6.76544	2.65094	1.398212
35	H	5.059163	2.212103	1.945852	76	H	-8.14578	1.961602	2.267436
36	H	3.78977	2.543878	3.155162	77	H	-8.30952	3.509555	1.430605
37	H	4.426093	3.872654	2.160826	78	C	-7.92355	2.649236	-1.15676
38	C	1.41273	1.030179	-3.60295	79	H	-8.36526	3.65107	-1.07985
39	H	1.542819	1.802314	-4.36792	80	H	-8.28076	2.206306	-2.09284
40	H	0.421796	1.117171	-3.15403	81	H	-6.83668	2.777977	-1.24358
41	H	1.497549	0.049643	-4.07898	82	C	-8.24118	-0.76378	-1.72306

Table S3, continued

#	atom	x	y	z	#	atom	x	y	z
83	H	-7.72696	-0.14807	-2.47775	125	H	-4.39711	-3.38136	2.729837
84	C	-9.757	-0.59816	-1.95377	126	H	-4.96863	-1.7318	2.343527
85	H	-10.0306	-0.94213	-2.95922	127	H	-3.64269	-1.97596	3.515397
86	H	-10.0851	0.443045	-1.86483	128	C	-4.05344	2.39067	-2.61275
87	H	-10.3404	-1.19193	-1.24059	129	H	-3.58362	2.016593	-3.52653
88	C	-7.82522	-2.22559	-1.97184	130	H	-4.33956	3.435589	-2.76751
89	H	-8.39432	-2.9172	-1.34243	131	H	-4.93663	1.793552	-2.38317
90	H	-6.761	-2.40037	-1.77132	132	C	-1.25984	-1.52514	-3.32928
91	H	-8.01857	-2.5072	-3.0151	133	H	-1.35757	-2.42834	-3.94007
92	C	-8.21356	-0.97277	1.543153	134	H	-0.30756	-1.53512	-2.79665
93	H	-7.62422	-0.50964	2.35043	135	H	-1.28402	-0.65393	-3.98928
94	C	-9.70207	-0.76387	1.886788	136	C	-4.15213	-1.23375	-3.23388
95	H	-9.94728	-1.25716	2.835968	137	H	-4.20578	-2.09338	-3.90887
96	H	-10.3574	-1.19491	1.121334	138	H	-4.04962	-0.32246	-3.8278
97	H	-9.96541	0.293809	1.991666	139	H	-5.06104	-1.16251	-2.63631
98	C	-7.87902	-2.47629	1.540216	140	C	-4.31078	1.307467	3.165156
99	H	-8.01849	-2.90324	2.541864	141	H	-4.26079	0.380449	3.740891
100	H	-6.84639	-2.67714	1.231387	142	H	-5.18963	1.272352	2.521047
101	H	-8.53707	-3.03076	0.862928	143	H	-4.37782	2.153225	3.856352
102	P	-2.67155	-1.40838	-2.0896	144	C	-1.42776	1.601374	3.415891
103	C	-2.81458	-3.20474	-1.4691	145	H	-1.57727	2.495097	4.030059
104	H	-3.28046	-3.80934	-2.25549	146	H	-0.44969	1.640578	2.933977
105	H	-1.79338	-3.57872	-1.33409	147	H	-1.46572	0.721818	4.064075
106	C	-3.61007	-3.3024	-0.16702	148	C	2.811097	-2.90847	1.963843
107	H	-3.64768	-4.33821	0.189107	149	H	3.265969	-3.39032	2.836553
108	H	-4.63694	-2.95238	-0.30571	150	H	1.78717	-3.28977	1.879349
109	P	-2.76957	1.472732	2.1017	151	C	3.614377	-3.20854	0.697561
110	C	-2.87926	3.267755	1.472047	152	H	3.644732	-4.28676	0.503239
111	H	-3.36705	3.878295	2.240406	153	H	4.643048	-2.84905	0.789584
112	H	-1.85164	3.634679	1.370138	154	C	3.498402	3.408015	-0.64699
113	C	-3.63074	3.365919	0.144465	155	H	3.448703	4.48199	-0.4343
114	H	-3.6488	4.400226	-0.21761	156	H	4.552606	3.141097	-0.76381
115	H	-4.66489	3.026573	0.251678	157	C	7.707253	2.764354	0.071572
116	C	-1.45592	-3.28715	1.845753	158	H	7.879928	2.788273	1.153706
117	H	-1.08165	-2.86696	2.782322	159	H	6.623478	2.752179	-0.09024
118	H	-0.63589	-3.32476	1.126205	160	H	8.099628	3.70355	-0.33938
119	H	-1.81776	-4.30212	2.03768	161	C	1.443925	3.536645	1.465023
120	C	-1.42013	3.321716	-1.80644	162	H	1.768304	4.578773	1.547465
121	H	-0.99927	2.872405	-2.70934	163	H	1.113116	3.193955	2.448646
122	H	-0.63691	3.382311	-1.04819	164	H	0.602897	3.471658	0.771369
123	H	-1.77259	4.329622	-2.04695	165	H	3.105301	3.597387	-2.77652
124	C	-4.09671	-2.33856	2.588907	166	H	1.652871	3.358375	-1.80115